Efficient black silicon solar cell with a density-graded nanoporous surface: Optical properties, performance limitations, and design rules

Hao-Chih Yuan, Vernon E. Yost, Matthew R. Page, Paul Stradins, Daniel L. Meier et al.

Citation: Appl. Phys. Lett. **95**, 123501 (2009); doi: 10.1063/1.3231438
View online: http://dx.doi.org/10.1063/1.3231438
View Table of Contents: http://apl.aip.org/resource/1/APPLAB/v95/i12
Published by the American Institute of Physics.

Efficient black silicon solar cell with a density-graded nanoporous surface: Optical properties, performance limitations, and design rules

Hao-Chih Yuan,[a] Vernon E. Yost, Matthew R. Page, Paul Stradins, Daniel L. Meier,[b] and Howard M. Branz
National Renewable Energy Laboratory, Golden, Colorado 80401, USA

(Received 3 August 2009; accepted 27 August 2009; published online 22 September 2009)

We study optical effects and factors limiting performance of our confirmed 16.8% efficiency "black silicon" solar cells. The cells incorporate density-graded nanoporous surface layers made by a one-step nanoparticle-catalyzed etch and reflect less than 3% of the solar spectrum, with no conventional antireflection coating. The cells are limited by recombination in the nanoporous layer which decreases short-wavelength spectral response. The optimum density-graded layer depth is then a compromise between reflectance reduction and recombination loss. Finally, we propose universal design rules for high-efficiency solar cells based on density-graded surfaces. © *2009 American Institute of Physics*. [doi:10.1063/1.3231438]

Low surface reflectance (R) of solar cells and detectors is needed to maximize the number of incident photons absorbed by the semiconductor that converts light to electrical energy. R is normally reduced in crystal Si and other solar cells with a quarter-wavelength antireflection (AR) coating applied to the top surface, although multilayer coatings have also been used to broaden the spectral width of the AR. Such AR coatings function by destructive interference of reflected waves and therefore normally have a narrow acceptance angle for AR at a given wavelength.

A density-graded surface layer can also suppress surface reflection and could replace conventional AR interference layers in Si solar cells, detectors and other photosensitive devices.[1] Such density-graded Si layers, often termed "black silicon" (bSi), can be based on a randomly nanoporous morphology[2–6] or on a "moth-eye" texture[7,8] composed of nanoscale periodic structures. A density-graded surface suppresses R exponentially as the grade depth, d, increases;[1,2] for $d \sim 500$ nm, $R < 2\%$ across the portion of solar spectrum converted by Si solar cells. Since it is not based on interference, bSi has a broad AR acceptance angle.[1,6,8] Because of the density grade, light at near-normal incidence escapes a bSi surface with little internal reflection. As in mirages and density-graded optical fibers,[9] however, light with angles larger than the critical angle ($\Theta_c \sim 10-16°$ from normal) is total internally reflected at a bSi/air interface, exactly as from a planar Si/air interface.

Demonstrations of bSi solar cells with efficiencies ranging from 8.8% to 13.9% were reported[5,6,10] but no systematic investigation of loss mechanisms was undertaken. In this letter, we analyze the optical and optoelectronic properties of 16.8% Si solar cells with nanoporous bSi layers we fabricate using our recently reported[2] one-step nanoparticle-catalyzed liquid etch. The issues that limit the efficiency of our cells represent significant challenges for developing high-efficiency solar cells with density-graded AR by any technique in any semiconductor material. After describing our methods and results on bSi devices, we present design rules for incorporating density-graded AR in solar cells.

We fabricate optical test structures and solar cells on 300 μm p-type double-side polished float-zone Si (100) substrates with resistivity of 2.7 Ω-cm. We produce bSi surfaces of various grade depths by immersing the Si substrate in 0.4 mM $HAuCl_4$ solution, adding an equal quantity of $HF:H_2O_2:H_2O$ 1:5:2 mixture, and soaking the wafer in a sonication bath for times from 1 to 8 min. Increasing the bSi etch time (t_e) increases d. Au nanoparticles are produced in the mixture and they catalyze subsequent nanoporous Si etching.[2] This method produces "double-sided bSi;" we also prepare "one-sided bSi" by protecting the back side during the bSi etching.[11] Residual Au on the surface is removed after the etch by sonicating in I_2/KI solution; however, secondary ion mass spectrometry (SIMS) analysis shows mid-10^{18} cm^{-3} of residual Au in the nanoporous layer. The Au concentration falls below the SIMS detection threshold of $\sim 10^{15}$ cm^{-3} within 0.5–1.0 μm from the surface. Hemispheric total R (R_{tot}) and transmittance (T_{tot}) for normal incidence are measured on a Varian Cary 6000i spectrophotometer with an integrating sphere. The spectrometer also provides the normal transmittance (T_{norm}).

Figures 1(a) and 1(b) show the $t_e = 3$ min spectral dependences of T_{tot} and R_{tot} for one-sided and double-sided bSi, respectively, with schematic insets showing the most important reflected and transmitted light rays. For both samples, R_{tot} is below 3% from 350 to 1000 nm wavelength, confirming the good AR properties of bSi. Figure 1(a) shows that T_{norm} of the one-sided bSi is lower than T_{tot} at weakly absorbed infrared (IR) wavelengths, indicating IR scattering in the top bSi surface (see inset). We also plot the transmission haze, $H_T = (T_{tot} - T_{norm})/T_{tot}$, with $H_T \sim 9\%$ at 1100 nm. About 90% of IR is transmitted through the back bSi/air interface [Fig. 1(b)] meaning that the scattering from the front must be mainly in the forward direction and within a cone defined by Θ_c.

Figure 2(a) and 2(b) show optical measurements on one-sided and double-sided bSi samples, respectively, at 1200 nm wavelength (where absorption is negligible), for $t_e = 0$ (planar) to 8 min. Figure 2(c) and 2(d) display cross-sectional scanning electron microscopy (XSEM) images after 3 and 6 min of bSi etching with $d \sim 500$ and 1000 nm, respectively.

[a]Author to whom correspondence should be addressed. Electronic mail: hao.chih.yuan@nrel.gov.
[b]Present address: Suniva, Inc., Norcross, GA 30092, USA.

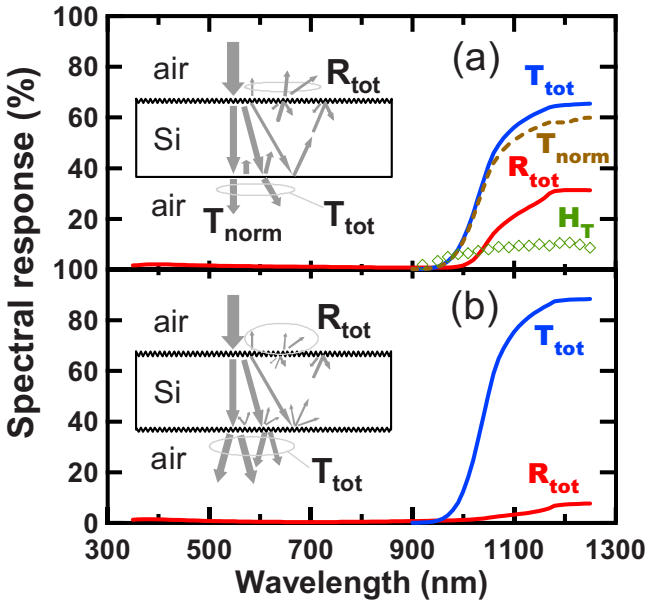

FIG. 1. (Color online) Spectral dependences of R and T for 3 min etched (a) one-sided and (b) double-sided bSi samples. Transmission haze (H_T) is also included in (a). The insets schematically show the main reflected and transmitted light paths.

Pixel-by-pixel computer analysis of a 3 min XSEM image shows a roughly linear grade in density, and therefore index of refraction. Images such as Figs. 2(c) and 2(d) show progressive development of larger lateral structures and etch-depth inhomogeneities with characteristic length scales reaching the IR wavelength in Si (~300 nm). These structures are presumably responsible for the increasing IR haze in Fig. 2(a) as t_e increases above 3 min. This IR scattering also increases R_{tot} with t_e in Figs. 2(a) and 2(b): there is progressively more back-scattering from the larger structures at the front bSi surface and also total internal reflection from the back due to the increasing fraction of light forward-scattered from the bSi front at angles greater than Θ_c. The low values of Θ_c in Si in combination with a diffuse back reflector are proven to lead to excellent light trapping in Si solar cells.[12] Therefore the bSi surface layer, with its total internal reflection, can provide efficient IR light trapping. As

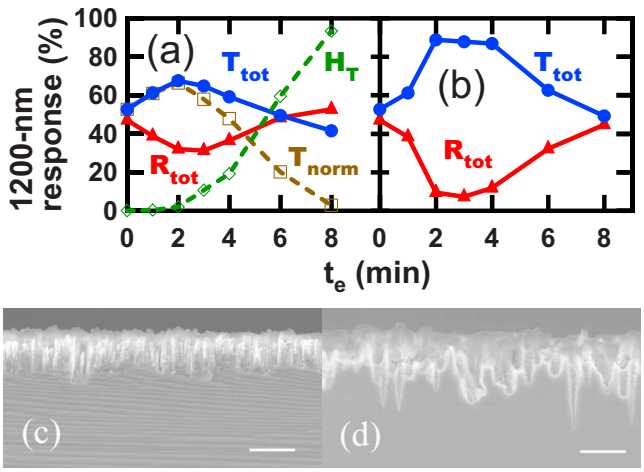

FIG. 2. (Color online) R and T at 1200 nm wavelength on (a) one-sided and (b) double-sided bSi samples, for black-etch times (t_e) from 0 (planar) to 8 min. Panels (c) and (d) present XSEM images of bSi surfaces with t_e=3 and 6 min, respectively. Scale bars are 500 nm.

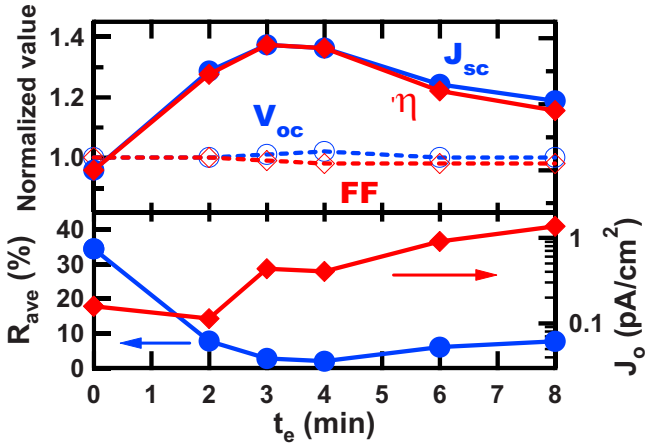

FIG. 3. (Color online) Performance comparison between planar (0 min etch) and bSi solar cells under 1-sun illumination, for black-etch times (t_e) up to 8 min.

a second-order effect, forward-scattering from inhomogeneities in the bSi layer may provide a photon path length increase that compensates for the escape through the graded-density front surface of the small amount of light reflecting from the diffuse back reflector at angles less than Θ_c.

We fabricate solar cells from one-sided bSi wafers and from double-side polished planar Si controls. We use standard processes to create a front phosphorous-diffused emitter and an Al back-surface field, as detailed in Ref. 11. A 20 nm thermal oxide is grown to passivate the black Si surface and improve blue response. We etch this oxide locally before evaporating a front metal grid. Illuminated current-voltage (IV) curves of photolithographically defined 1 cm^2 cells are measured with calibrated 1-sun simulators. Our best bSi solar cell is made with t_e=3 min and is independently confirmed at NREL to have efficiency (η) of 16.8%, with open-circuit voltage (V_{oc}) of 612 mV, short-circuit current (J_{sc}) of 34.1 mA/cm^2 and fill factor (FF) of 80.6%. This exceeds by 2.9% the highest previously reported efficiency of 13.9% for a Si solar cell[6] without any deposited AR coating.

Figure 3 shows the 1-sun IV parameters for bSi solar cells normalized to the planar control cell, the saturation current density (J_o) extracted from the illuminated IV,[13] and the average R weighted by solar photon flux (R_{ave}) from 350 to 1000 nm wavelength, versus t_e. All of our bSi solar cells have V_{oc} and FF comparable to the planar cell, suggesting little problem in making contact to the nanoporous top surface. The increase in J_o indicates increasing recombination in the thickening nanoporous layer.

Figure 4 shows the internal quantum efficiency (IQE) on planar, 3, 4, and 6 min etched bSi solar cells (lines) together with the results from our modeling with the one-dimensional device program PC1D (symbols). There is a reduction in bSi-cell IQE below ~700 nm wavelength and it worsens with increased t_e. Integration of the blue IQE loss for the 3 min bSi cell shows a J_{sc} loss of 3.6 mA/cm^2. However, the cell has R_{ave}=2.7%, corresponding to a loss of only ~1 mA/cm^2, less than conventional AR coatings. We were unable to model the IQE of the bSi cells with any combination of poor planar front-surface recombination velocity and reduced bulk lifetime. Instead, we model the IQE well by assuming that the bSi nanoporous layer acts as a low-lifetime "dead layer" which is thinner (Fig. 4 legend) than d. We

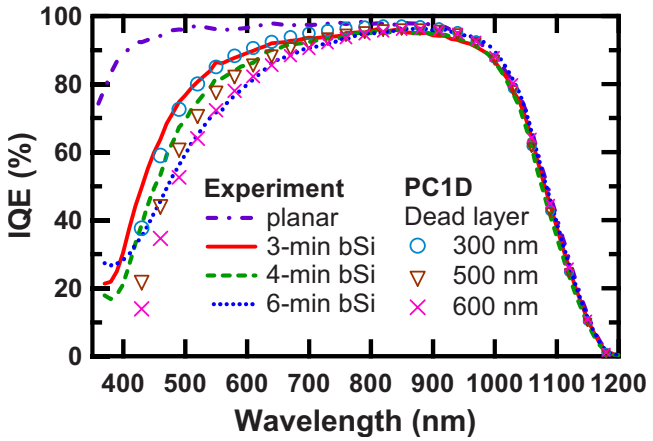

FIG. 4. (Color online) IQE of planar and bSi solar cells. Symbols show PC1D calculations of IQE assuming highly doped surface dead layers of the indicated thicknesses.

implement the nanoporous dead layers as a heavily doped Si (10^{21} cm^{-3} of P) with high Auger recombination. We attribute the dead layer to high doping concentration in the nanoporous layer and additional recombination at the enormous internal surface, perhaps exacerbated by residual Au contamination. Light scattering on the nanoporous layer may increase photon path lengths inside the dead layer and worsen IQE loss. The 4 min bSi cell has a better R_{ave} = 1.9%, but a thicker dead layer than the 3 min cell (Figs. 3 and 4). The ~500 nm nanoporous grade depth of our optimized 3 min bSi cell represents a compromise between AR and recombination. Figure 4 also shows that the IQE from 1000 to 1200 nm is not higher in the bSi than in the planar control, despite the forward-scattering of IR from our bSi surfaces. Our planar control and bSi cells all have Al-paste alloyed back surfaces that are normally effective light scatterers.[14] The effective diffuse reflection from the back side, together with excellent light trapping at the front Si/air interfaces, evidently results in little difference in IR optical path length between the two cells.

Our work leads us to suggest four design rules for solar cells based on nanostructured density-graded layers: (1) good AR requires a deep density grade depth, d. However, d must be kept as small as possible to avoid excess surface recombination in the nanoporous layer. (2) Increasing the characteristic nanoscale dimension, δ, (in this case, the pore diameter) reduces the surface area for dopant in-diffusion and for recombination because nanostructures of a given mass density have a surface area that scales as $1/\delta$. However, δ must be less than the smallest wavelength of light of interest so that the nanoporous layer acts as a laterally homogenous density-graded layer and minimizes back-scattering that increases R.[2] With $n \sim 6$ in Si in the 380–400 nm range, the nanoscale dimension should probably be less than ~60 nm. (3) The back-surface of the cell must reflect weakly absorbed light at angles greater than Θ_c to avoid the efficient escape of near-normal light from the density-graded front surface. (4) The method of fabricating the nanostructured density-graded layer must be inexpensive, such as our one-step liquid etch.

In summary, a simple, one-step, nanoparticle-catalyzed bSi etch can provide effective AR for efficient Si solar cells, without reducing V_{oc} or FF. The IQE falls significantly at short wavelength as the bSi etch time increases, due to high doping and/or surface recombination in the nanostructured density-graded layer. Although the density-graded layers provide little internal reflection of near-normal light, a diffuse back-reflector, scattering at bSi nanoporous surfaces, and total internal reflection from bSi above the critical angle leave the IR IQE little changed from a planar control. A 3 min bSi etch, producing a density grade about 500 nm deep, provides the best compromise between surface reflection and blue IQE loss: we fabricate a 16.8% Si solar cell without any deposited AR coating.

This work was supported by the U.S. Department of Energy under Grant No. DE-AC36-08GO28308. We thank Anna Duda, Lorenzo Roybal, Bobby To, Robert Reedy, and Paul Ciszek for cell fabrication and characterization assistance.

[1] R. B. Stephens and G. D. Cody, Thin Solid Films **45**, 19 (1977).
[2] H. M. Branz, V. E. Yost, S. Ward, K. M. Jones, B. To, and P. Stradins, Appl. Phys. Lett. **94**, 231121 (2009).
[3] M. Y. Shen, C. H. Crouch, J. E. Carey, and E. Mazur, Appl. Phys. Lett. **85**, 5694 (2004).
[4] X. Li and P. W. Bohn, Appl. Phys. Lett. **77**, 2572 (2000).
[5] L. Stalmans, J. Poortmans, H. Bender, M. Caymax, K. Said, E. Vazsonyi, J. Nijs, and R. Mertens, Prog. Photovoltaics **6**, 233 (1998).
[6] H. Sai, H. Fujii, K. Arafune, Y. Ohshita, Y. Kanamori, H. Yugami, and M. Yamaguchi, Jpn. J. Appl. Phys., Part 1 **46**, 3333 (2007).
[7] S. J. Wilson and M. C. Hutley, Opt. Acta **29**, 993 (1982).
[8] Z. Yu, H. Gao, W. Wu, H. Ge, and S. T. Chou, J. Vac. Sci. Technol. B **21**, 2874 (2003).
[9] M. Young, *Optics and Lasers*, (Springer, Berlin, 1993), p. 261.
[10] S. M. Vernon, N. M. Kalkhoran, H. P. Maruska, and W. D. Halverson Proceedings of the 24th IEEE Photovoltaic Specialist Conference, 5–9 December 1994 (unpublished), pp. 1583–1586; A. Krotkus, K. Grigoras, V. Pacebutas, I. Barsony, E. Vazsonyi, M. Fried, J. Szlufcik, J. Nijs, and C. Levy-Clement, Sol. Energy Mater. Sol. Cells **45**, 267 (1997); S. Koynov, M. S. Brandt, and M. Stutzmann, Phys. Status Solidi **1**, R53 (2007).
[11] H.-C. Yuan, V. E. Yost, M. R. Page, L. Roybal, B. To, P. Stradins, D. L. Meier, and H. M. Branz, Proceedings of the 34th IEEE Photovoltaic Specialist Conference, 7–12 June 2009 (unpublished).
[12] A. Goetzberger, Conference Record of the 15th IEEE Photovoltaic Specialist Conference, May 1981, (unpublished), pp. 867–870.
[13] K.-I. Ishibashi, Y. Kimura, and M. Niwano, J. Appl. Phys. **103**, 094507 (2008).
[14] A. Ristow, M. Hilali, A. Ebong, and A. Rohatgi, Proceedings of the 17th European Photovoltaic Solar energy Conference, Munich, Germany, October 2001, (unpublished), pp. 1335–1338.